Fuel 235 (2019) 63–71

Contents lists available at ScienceDirect

Fuel

journal homepage: www.elsevier.com/locate/fuel

Full Length Article

Visualization study on the promotion of natural gas hydrate production by water flow erosion

Bingbing Chen, Mingjun Yang*, Huiru Sun, Pengfei Wang, Dayong Wang

Key Laboratory of Ocean Energy Utilization and Energy Conservation of Ministry of Education, Dalian University of Technology, Dalian 116024, China

ARTICLE INFO

Keywords:
Methane hydrate
Water flow
Hydrate distribution
Hydrate exploitation

ABSTRACT

Natural gas hydrates (NGHs) are a new, clean, and effective energy source with great potential for exploitation. The efficient exploitation of NGHs has been a focus of research worldwide. Water migration in hydrate sediments is an important parameter influencing NGH exploitation. However, there is still little research in terms of visualization studies on the variation of hydrate distribution during the water flow process in hydrate-bearing sediment. Such variation of hydrate distribution and the influence of water migration on methane hydrate (MH) dissociation with different backpressures and water flow rates were systematically and visually analyzed in this study, where the influence of temperature and pressure variation on MH dissociation was completely eliminated. The results showed that the chemical potential difference between the hydrate phase and the aqueous phase caused MH dissociation during the water flow process and that the rate of MH dissociation increased with decreasing backpressure and increasing water flow rate. When the rate of MH dissociation is low, there will be a longer time for the flow channel to appear, vary, and disappear. Based on this conclusion, a new method of water flow erosion to improve NGH exploitation is proposed in this study.

1. Introduction

With the development of human society, the global energy demand is predicted to increase rapidly in the coming decades [1,2]. Nowadays, traditional fossil fuels such as oil and coal comprise approximately 85.9% of the global energy supply [3]. It is essential to find a sustainable alternate energy source to meet the continuously increasing energy demand with the decrease of traditional fossil fuels [2,4]. Natural gas hydrates, which are widely distributed in continental permafrost or marine sediment, are regarded as an alternative energy resource in consideration of their high energy density and purity [3,5,6]. In past decades, natural gas hydrates (NGHs) have attracted worldwide attention for investigation.

NGHs are crystalline solids composed of methane molecules and water molecules under low-temperature and high-pressure conditions [7–9]. The hydrate thermodynamic equilibrium is affected by temperature, pressure, chemical potential differences, and chemical potential correction caused by the dissolution of guest molecules in pure water [10]. All known hydration decomposition methods are based on shifting the thermodynamic equilibrium of the system [11]. There are mainly four methods of NGH exploitation, as follows: (1) depressurization [12–14], (2) thermal stimulation [15], (3) CO_2 replacement [16–18], and (4) inhibitor injection [19–21]. These four methods are mainly based on the temperature and pressure variations.

In past years, some measurements of NGH exploitation have been performed. The depressurization method has been widely used to liberate natural gas from methane hydrate (MH) reservoirs as a cost-effective solution because it does not require external energy [22]. However, the depressurization method has a low methane production rate, and the endothermic hydrate dissociation reaction may result in secondary hydrate formation [23]. In order to study changes during the hydrate dissociation process induced by depressurization, Yousif et al. [24,25] studied the process of hydrate dissociation in Berea sandstone by depressurization, and they derived a three-phase boundary model to describe the dissociation process. Kono et al. [26] studied the kinetic dissociation rate of hydrates using the depressurization method and found that sediment properties had a significant effect on the dissociation rate. Sloan [27] and Konno et al. [28] studied the characteristics of gas production from oceanic MH reservoirs by the depressurization method and both found that the effective permeability and initial temperature of the reservoirs were important factors of gas production. Regarding the other three NGH exploitation methods, Kawamure [29] studied the hydrate dissociation kinetics by dissociating pellet-shaped samples, which mimic naturally occurring hydrates in ocean sediments, with a viscous fluid or pure water at different temperatures. Tang et al. [30] concluded that the gas production rate

* Corresponding author.
E-mail address: yangmj@dlut.edu.cn (M. Yang).

https://doi.org/10.1016/j.fuel.2018.07.072
Received 2 April 2018; Received in revised form 18 June 2018; Accepted 18 July 2018

increases with increasing time until it reaches a maximum and then it starts to decrease but that the water production rate remains nearly constant during the gas production process. They also found that the energy ratio of thermal stimulation generation can be affected by the hydrate content of the sediment, the flow rate, and the water injection temperature. Sun et al. [31] suggested that liquids flowing in the well may lose the most heat, resulting in an obvious decrease in the heat impact. Komai et al. [32] measured the replacement rate between CO_2 and CH_4 occurring in a CH_4 hydrate using in situ Raman spectroscopy, and they found that CO_2 hydrates coexisted with the CH_4 hydrate phase and were generated at both the surface and inside the CH_4 hydrate samples and ice crystals. Geng et al. [33] simulated methane dynamics by using carbon dioxide molecules to replace methane molecules in the hydrate in order to assess the possibility of methane reformation. Mutalik et al. [34] carried out a series of experiment on the depressurization and injection of a hot saline solution. Li et al. [35] studied gas production from MHs through injecting hot brine at different temperatures and concentrations, and found that the concentration and temperature changed the gas production yield.

Irrespective of the type of NGH exploitation method, such methods have always been accompanied by water migration. Many investigations have researched the NGH exploitation process, but thus far, there has been no visualization study on the variation of hydrate distribution and the influence of water migration on MH dissociation in hydrate-bearing sediment during the water flow process. In addition, there are few reports systematically analyzing the influence of the chemical potential difference on MH dissociation. Furthermore, it was found that higher water production has a negative influence on the gas production efficiency irrespective of the exploitation method used [36–38]. Reducing water production is hence very important for hydrate exploitation. In this study, in order to avoid high water production, which leads to low hydrate exploitation rate and efficiency, we considered this problem in terms of excess water, chemical potential difference, and the transfer of heat and mass. We proposed a new method of water flow erosion in which the temperature is lower than phase equilibrium temperature and the backpressure higher than phase equilibrium pressure, to completely eliminate the influence of temperature and pressure variations on MH dissociation. The four main purposes of water flow erosion are as follows: (1) inducing and increasing the chemical potential difference between the water and hydrate phases; (2) enhancing the heat and mass transfer of the hydrate reservoir; (3) increasing the salinity of the hydrate reservoir; and (4) inhibiting the secondary hydrate formation. All these purposes are achievable and promote efficient hydrate decomposition. This investigation thus achieved visualization research by MRI, which is considered as a reliable technology to aid hydrate research and has been used for many years [39]. The experiment results may provide guidance for investigating NGH exploitation.

2. Experiments

2.1. Apparatus and materials

A schematic diagram of the experimental system is shown in Fig. 1. The experimental apparatus shown in Fig. 1 was designed to investigate methane hydrate (MH) dissociation during the water flow process. Xiao-Sen Li et al. [40] found that hydrates will dissociate during water injection and that low-speed flow slightly affects the hydrate dissociation. A magnetic resonance imaging (MRI) system (Varian, Inc., Palo Alto, CA, USA) for visualizing the MH dissociation during the water flow process formed the core component of the experimental system. The resonance frequency of this system with a 9.4 T magnet field intensity was 400 MHz. Two-dimensional (2D) proton density-weighted images were obtained by a standard spin echo pulse sequence that was chosen in this study. The sequence parameters were as follows: echo time (TE) = 4.39 ms, image data matrix = 128 × 128, and the field of view (FOV) = 30 mm × 30 mm (2.0 mm in thickness). The sequence acquisition time was 2.14 min for one image.

A high-pressure vessel capable of withstanding a pressure of 15 MPa and made of a nonmagnetic material (polyimide) was used in this study. The effective size of the vessel was 15 mm in diameter and 200 mm high. The high-pressure vessel was surrounded by a jacket, which was used to cool the vessel via a circulator bath. Three thermostat baths (FL300 and FL 25, JULABO, Seelbach, Germany) were used to control the temperature of the MRI machine, the high-pressure vessel, and the injection pump. Three high-precision syringe pumps (260D, Teledyne Isco Inc., Lincoln, NE, USA) were used to inject methane gas and deionized water, and to control the backpressure in the experiment. Two pressure transducers (3510CF, Emerson Electric Co., Ltd., St. Louis, USA) were connected to the input and output of the high-pressure vessel. A differential pressure sensor (Nagano Keiki, Japan, with an accuracy of ± 0.01 kPa) installed at both ends of the reactor was used to acquire pressure difference signals. The signals acquired from the pressure transducer and the pressure difference signals were collected and processed by the A/D module (Advantech Co., Ltd., Milpitas, CA, USA). Glass beads (As-One Co., Ltd., Japan) with particle diameters of 0.177–0.250 mm (BZ02) mm and a porosity of 35.4% were used as the homogeneous skeleton structure of the porous medium. CH_4 (Dalian Special Gases Co., Ltd., China, with a purity of 99%) was used as the gas source. Deionized water was used in all the experiments.

2.2. Hydrate formation

The glass beads were used to tightly fill the vessel. Then the vessel was placed into the center of the MRI magnet and connected to the experimental system. The volume of the vessel was 12.51 mL, and the porosity of the glass beads was 35.4%. Next, deionized water was injected into the vessel under a constant pressure of 1000 kPa after the vessel was vacuumed. Then, the deionized water was pressurized to 6000 kPa to saturate the porous media and this pressure was maintained for 1 h. The deionized water was displaced by high-pressure CH_4 and the volume of displaced water was used to calculate the initial water saturation. Then, the vessel was pressurized to 6000 kPa with CH_4 gas and kept stable during the hydrate formation process. The thermostat bath was set to 274.15 K and kept stable throughout the experiment. MRI images were continuously obtained during the experiment.

2.3. Water flow process

There were sixteen experimental cases in this study. The water injection conditions and results for the sixteen cases are shown in Table 1. Case 1 was chosen to show the water flow process. After complete hydrate formation, the high-pressure vessel and backpressure pump were interconnected and the backpressure valve was set to 3200 kPa. During the backpressure adjustment, the backpressure was first set to 5000 kPa, and then it was set to 4000 kPa, and 3500 kPa. Finally, it was set to 3200 kPa and kept stable at that pressure for a period to ensure that there was no hydrate dissociation. The equilibrium pressure was 2980 kPa at a temperature of 274.15 K, as calculated by CSMHyd [4]. Thus, the hydrate remained stable and there was no dissociation during the changing of backpressure. Then, the water injection pump, which was set to the same pressure as the backpressure pump, was interconnected to the high-pressure vessel and the water temperature was set to 273.65 K to prevent hydrate dissociation. The hydrate-saturated sediment core was saturated with cooled deionized water injected at a velocity of 2 mL/min. Then, the cooled deionized water was continuously injected into the vessel with a velocity of 10 mL/min. Images were continuously obtained throughout the water flow process and the time interval was 2 min.

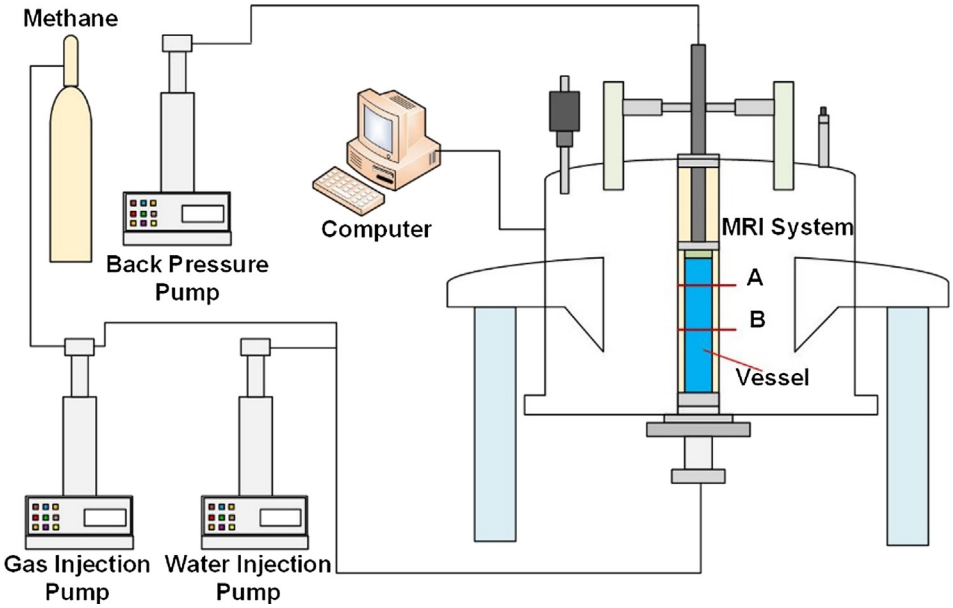

Fig. 1. Schematic of the experimental system.

3. Results and discussion

A new method of water flow erosion for NGH exploitation was used in this study. Sixteen experimental cases were investigated in this study. The hydrate saturation was controlled to approximately 18.5%, and the specific experimental conditions are shown in Table 1. Flow velocities of 10, 2, 1.5, 1, 0.5, 0.2, and 0.1 mL/min were used in this investigation. The backpressure was set to 3200, 3300, and 6000 kPa, corresponding to each water flow rate. The whole water flow process was recorded by MRI. What needs to be emphasized is that there was no increase in temperature or depressurization throughout the water flow process. The hydrate saturation was calculated by the mean intensity (MI) data, and the estimating equation [41,42] was as follows:

$$S_h = 1.25\frac{(I_0 - I_i)\cdot S_{w0}}{I_0} * 100\% \quad (1)$$

where S_{w0} is the initial water saturation and I_0 and I_i are the MI values of the liquid solution at the initial time and at time i (min). Both the saturation and MI values are dimensionless.

3.1. Obvious promotion of MH hydrate dissociation during the water flow process

Sixteen experimental cases were investigated in this study, which were used to research the variation of MH distribution and dissociation during continuous water flow using different water flow rates and different pressures. In this study, case 16, with a flow rate of 0.1 mL/min and a backpressure of 3200 kPa, was used to prove the viability and effectiveness of water flow erosion promotion. Fig. 2 shows the variation of MH distribution and dissociation during the continuous water flow at a flow rate of 0.1 mL/min and a backpressure of 3200 kPa. As shown in Fig. 2, the image at 0 min shows the hydrate-saturated sediment core immediately after water saturation. Compared to the image at 0 min, the image was brighter at 200 min and there was little change before 600 min. A small bright white zone appeared at 600 min because the hydrate dissociated in this small zone, and the pores in this dissociation zone were completely saturated by water. The size of the bright white zone gradually increased, and the increase along the axis was especially obvious at 680, 720, and 740 min. The size of the bright white zone became increasingly larger, and a flow channel was formed at the period of 740–2000 min. The variation of the flow channel slowed at the period of 2000–2200 min. The MH dissociated in the bottom of the hydrate-saturated sediment core at 2200 min, and the dissociation zone became bright white. Almost all the MH in the bottom of the hydrate-saturated sediment core dissociated at 2800 min. With the continuous flow of water, the MH in the hydrate-saturated sediment core completely dissociated at 3600 min, and the whole image became bright white.

Fig. 3 shows the variation of MI and water saturation increment during the water flow process with a flow velocity of 0.1 mL/min. As shown in Fig. 3, there was the same variation trend between water saturation and MRI mean intensity. Thus, the variation of MRI mean intensity also reflected the variation of water saturation increment in the hydrate-saturated sediment core. As shown in Fig. 3, there was a rapid increase in the water saturation increment at the initial stage of water flow, with little variation beyond 0.061 in this experimental cage. When the flow channel appeared at 660 min, there was a sudden increase in water saturation increment. When the water saturation increment reached 0.119 in this cage, it began to show a slowly increasing trend. This is because the dissociation zone was completely

Table 1
Experimental conditions and results.

Experiment number	1	2	3	4	5	6	7	8	9
Hydrate saturation (%)	18.4	18.1	18.6	18.5	18.3	19.0	18.4	18.7	18.3
Flow velocity (mL/min)	10			2			1.5		
Backpressure (kPa)	3200	3300	6000	3200	3300	6000	3200	3300	6000
Experiment number	10	11	12	13	14	15		16	
Hydrate saturation (%)	18.1	17.9	18.4	18.6	18.3	18.5		18.6	
Flow velocity (mL/min)	1.0			0.5		0.2		0.1	
Backpressure (kPa)	3200	3300	6000	3200	3300	3200		3200	

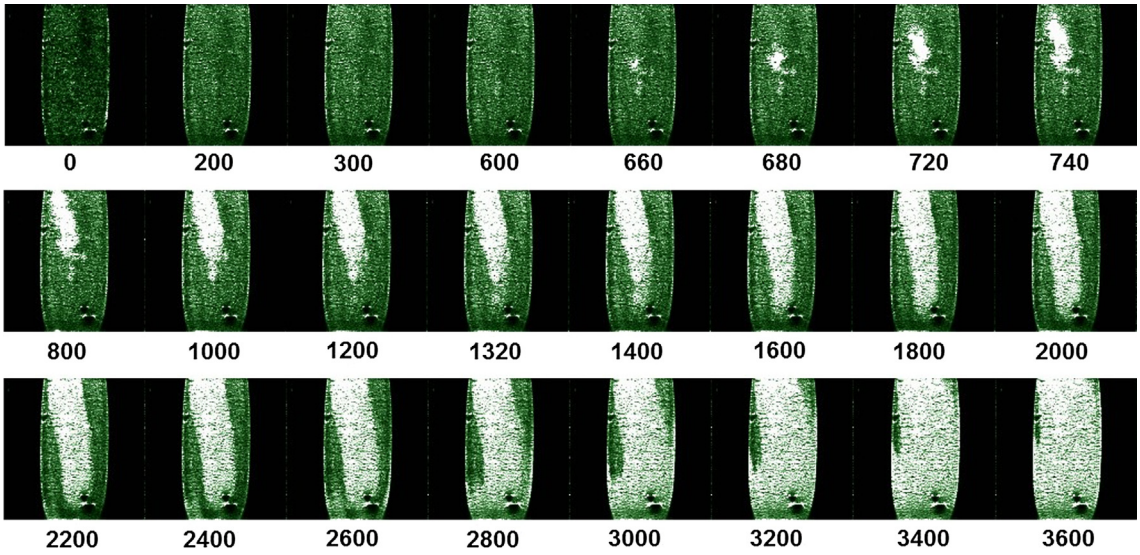

Fig. 2. Changes in the dissociation and distribution of MH during the water flow process with a flow velocity of 0.1 mL/min.

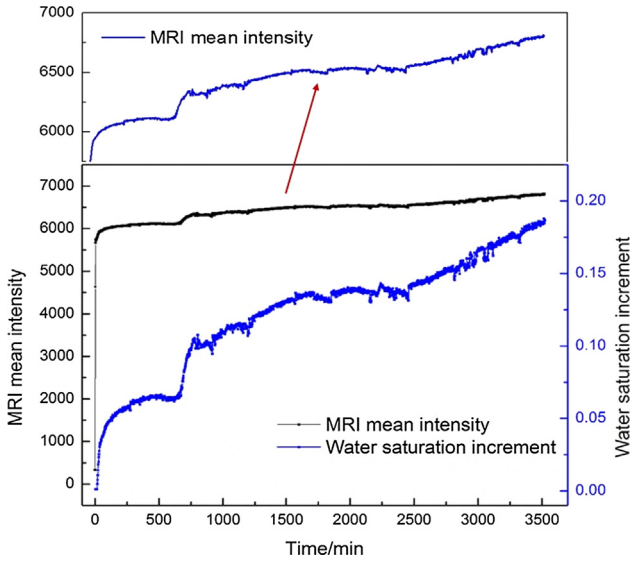

Fig. 3. Variation of MI and water saturation increment during the water flow process with a flow velocity of 0.1 mL/min.

saturated with water when almost all the MH in this zone dissociated completely and the flow channel formed completely. Therefore, there was a sudden increase of water saturation increment. Also, there was a slowly increasing trend at 1500–2400 min. This was because the MH dissociated slowly along the two sides of the flow channel in the continuous water flow process.

The reasons for MH dissociation during the water flow are as follows. MH forms an unstable cage complex, and there was dynamic equilibrium under the condition of water enrichment. After MH formed completely, there was a dynamic equilibrium in terms of mass transfer between the water and hydrate phases, and so the chemical potential difference, also called the Gibbs free energy difference, was zero. So, there was no MH dissociation. In the water flow process, the flowing water was cooled to 273.65 K and the backpressure was set to 3200 kPa as compared to those of the MH formation condition, in which the formation temperature was set to 274.15 K and the equilibrium pressure was 2980 kPa at this temperature. The water flow pressure and temperature were in the thermodynamic stability region of the hydrate, which ensured there was no MH dissociation caused by the variation of pressure and temperature. Thus, the MH dissociation was completely caused by the chemical potential difference. Sean et al. also pointed out that the main reason for MH dissociation was the chemical potential difference [43], which was converted to the concentration of methane dissolved in the aqueous phase in their study. There were two reasons for the small bright white zone at 600 min. The first one was maldistribution of MH in the hydrate-saturated sediment core. When the hydrate-saturated sediment core was saturated by water, in the lower hydrate saturation zone, the water saturation was significantly higher, and so the chemical potential difference was higher than that in the zone with higher hydrate saturation. Thus, because of the imperviousness of the hydrate [44], the higher hydrate saturation zone was better able to maintain the stability of the MH. However, some methods are used to ensure the uniform distribution of MH in hydrate-saturated sediment core, such as uniform sand filling, the stable process of gas injection, and water displacement before hydrate formation. However, there were also other factors that caused the maldistribution of MH. The second reason for the small bright white zone at 600 min was the maldistribution of temperature because of the water flow process. An increase of local temperature will accelerate the dissociation of MH. Taken together, a small bright white zone appeared at 600 min. With the dissociation of MH, the permeability of the bright white zone and its surrounding zone increased and the water mobility was better. Thus, MH will dissociate along the two sides of the flow channel in the continuous water flow process.

Based on the above experimental research, a new method of water flow erosion is proposed to promote natural gas hydrate production.

3.2. *Influence of backpressure and flowrate on MH hydrate dissociation*

Fig. 4 shows the variation of MI during the water injection with different backpressures under the same flow velocity. As mentioned above, the variation of MI during water injection was reflected in the variation of water saturation in the hydrate-saturated sediment core. Therefore, the variation of MI will continue to be used to show the reach in the flowing section. As shown in Fig. 4, the variation of MI showed the same trend as that in Fig. 3. At one moment, the MI sharply decreased and then slowly increased again, until the MI reached the value at which no hydrate existed. With increasing MI, the water saturation in the pores also increased. The period of 0–4 min represents the water saturation process for all the experimental cases. After the water saturation process, the water flow rate was set to the experiment design conditions, which were 0.5, 1.0, 1.5, 2, and 10 mL/min. At each water flow rate, the backpressure during the water flow was set to

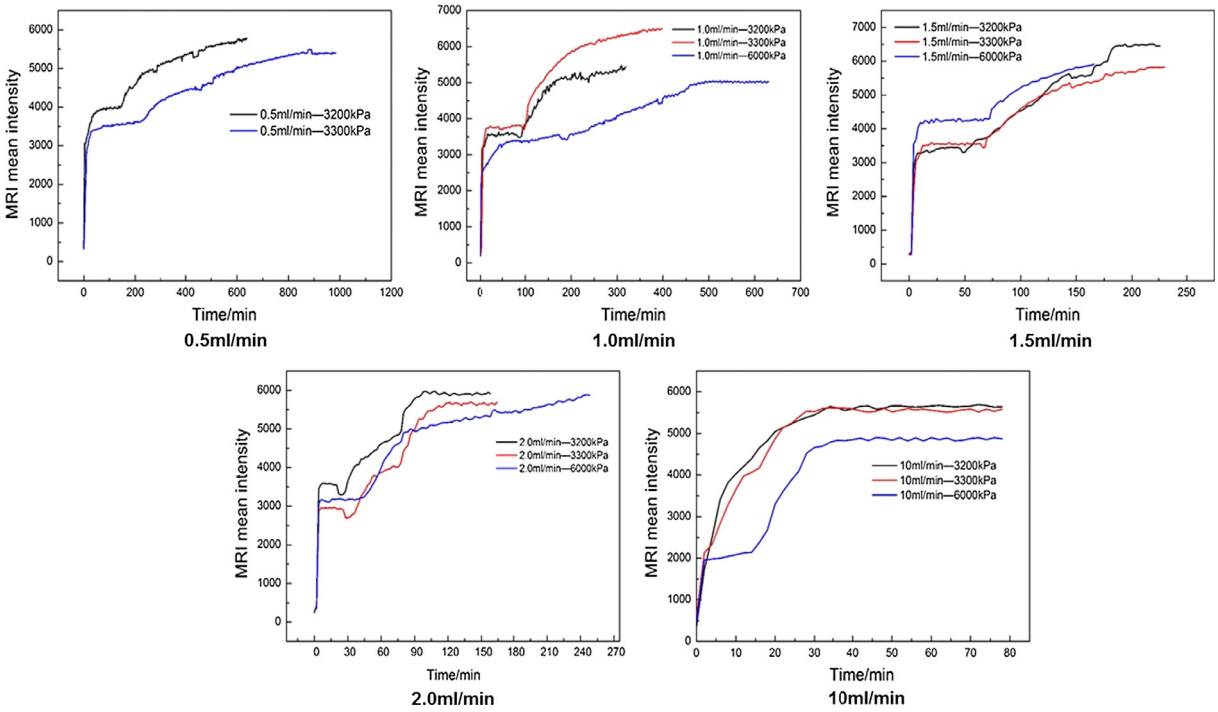

Fig. 4. Variation of MI during water injection with different backpressures under the same flow velocity.

3200, 3300, and 6000 kPa. As shown in Fig. 4, the time of hydrate stability increased with increasing backpressure. Then there was a sharp decrease before a slow increase at flow rates of 1.0, 1.5, and 2.0 mL/min. This is because the hydrate started to dissociate, and the dissociation gas induced to the migration of free water in the surrounding hydrate dissociation zone. When the backpressure was 6000 kPa, there was no sharp decrease. This was because the hydrate remained stable with the higher backpressure and the amount of dissociation gas was not sufficient to cause free water migration. The influence of chemical potential difference on hydrate dissociation decreased. When the flow rate was 0.5 mL/min, there was also no sharp decrease. This was because the dissociation gas was displaced to the backpressure pump by flowing water during the water flow process. A smaller water flow rate reduced the variation of the concentration of methane dissolved in the aqueous phase, and so the rate of MH dissociation was slow. Also, the amount of dissociation gas was not sufficient to cause free water migration. As shown in Fig. 4, the MH dissociated completely at 30 min at a flow rate of 10 mL/min, which indicates that the flow rate also had an influence on MH dissociation. This was because the dissociation gas was more quickly displaced to the backpressure pump by flowing water with a higher flow rate, which reduced the variation in the concentration of methane dissolved in the aqueous phase. Accordingly, the higher the flow rate, the faster the MH dissociation rate.

Figs. 5–9 show the distribution change for MH during the continuous water injection with water velocities of 10, 2.0, 1.5, 1.0 (Figs. 5–8, respectively) and 0.5, 0.2, and 0.1 mL/min (Fig. 9) and backpressures of 3200, 3300, and 6000 kPa. In the figures, rows A, B, and C correspond to experimental conditions with backpressures of 3200, 3300, and 6000 kPa, respectively. As shown in the figures, the variation of distribution changes for MH during the continuous water flow process shows the same trend. In the continuous water flow process, a small bright white zone appeared first, indicating that most of the MH had been dissociated. The flow channel gradually grew along the axis, becoming larger and larger along the two sides of the flow channel until the flow channel disappeared in the hydrate-saturated sediment core. Comparing the distribution changes for MH in the figures, it is apparent that it takes longer for the flow channel to appear and that it varies and disappears faster with increased backpressure at the same flow rate. There was low MH dissociation at first, and water preferentially flowed through this initial dissociation zone under the action of capillary power [45]. The rate of MH dissociation will increase with increasing hydrate-phase porosity [46].

As shown in Figs. 5–9, there will be a shorter time for the flow channel to appear, vary, and disappear with increasing water flow rate at the same backpressure. As shown in Fig. 5, the flow channel appeared at 2 min and disappeared at 20 min with a water flow rate of 10 mL/min and a backpressure of 3200 kPa. As shown in Fig. 10, the flow channel appeared at 660 min and disappeared at 3600 min with a water flow rate of 0.1 mL/min and a backpressure of 3200 kPa. This is because the dissociation gas decreased the chemical potential difference, which caused the slow dissociation of MH. The dissociation gas was displaced to the backpressure pump rapidly with higher water flow rates, and there was little concentration of methane dissolved in the aqueous phase. Furthermore, in the water flow erosion method, where continuous water flow is maintained during hydrate exploitation process, the gas from hydrate decomposition is replaced by flowing water. Thus, there will be faster heat and mass transfer in the hydrate-saturated sediment core with a higher water flow rate, which results in higher chemical potential differences and provides greater driving force for inducing hydrate decomposition and greatly improving the hydrate exploitation efficiency [47–49]. Thus, there was a rapid dissociation rate of MH. As shown in Fig. 5, it can be predicted that there will be no change in the rate of hydrate dissociation, the appearing and disappearing time of the flow channel, and the dissociation zone of MH when the water flow rate reaches a value of more than 10 mL/min. This prediction is the same for other experimental conditions with different backpressures.

3.3. Generation and variation of flow channel in MH dissociation process

As shown in Figs. 5–9, the flow channels appeared at one moment with different backpressures and different water flow rates, and there were four stages for the distribution of MH in the hydrate-saturated sediment core during the continuous water flow process. The first stage was the stability of the hydrate reservoir. In this stage, no obvious flow

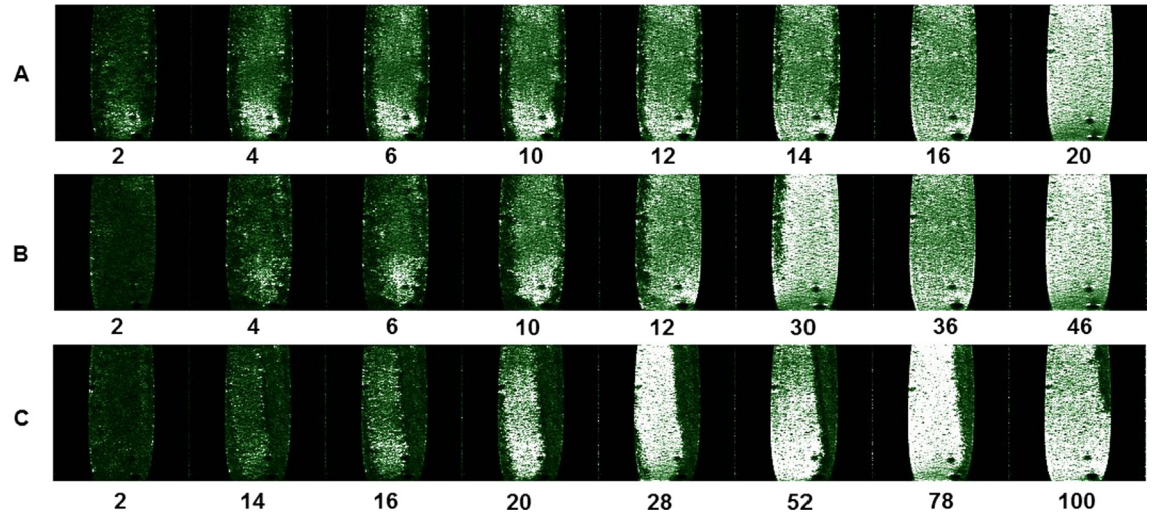

Fig. 5. Distribution changes for MH during water injection with a water velocity of 10 mL/min and under backpressures of 3200, 3300, and 6000 kPa.

channel appeared because of the higher concentration of methane dissolved in the aqueous phase. Also, the dissociation gas was not displaced to the backpressure pump completely, and so the MH dissociated slowly. The second stage was the local dissociation of MH. In this stage, a bright white zone appeared because of the maldistribution of MH in the hydrate-saturated sediment core [50]. The permeability was better in the zone with lower hydrate saturation. Thus, the displacement of dissociation gas was easier and the chemical potential difference was higher in this zone. The third stage was the formation of flow channels. In this stage, the bright white zone gradually grew along the axis until the flow channel formed because of the influence of capillary force. The water will flow through this zone preferentially. The fourth stage was the expansion and disappearance of the flow channel. In this stage, the size of flow channel increases along the two sides of itself until the flow channel disappears. The chemical potential difference at the junction of the water and hydrate phases was bigger than that of other zones, and so the MH dissociated along the two sides of the flow channel. However, there was a water film that protected the stability of MH [51] at the junction of the water and hydrate phases during the water flow process. As shown in Figs. 5–9, the times of the appearance and duration of the four stages were different with different backpressures and different water flow rates. Therefore, efficient MH exploitation is influenced by reservoir pressure and water flow rate.

Fig. 10 shows the time at which the flow channel appears during the continuous water flow process. Fig. 11 shows the time at which the flow channel disappears during the continuous water flow process. When there was a sudden increase of MRI mean intensity, as shown in Fig. 4, a small bright white zone appeared, as shown in Figs. 5–9, which was the moment the flow channel appeared. When there was no significant change of MRI mean intensity, as shown in Fig. 4, the whole image became bright white, as shown in Figs. 5–9, which was the moment the flow channel disappeared. As shown in Fig. 10, the appearing time changed exponentially. It will take longer for the flow channel to appear with increasing backpressure and decreasing water flow rate. As shown in Fig. 11, the disappearing time also changed exponentially. It will take longer for the flow channel to disappear with increasing backpressure and decreasing water flow rate. As shown in Figs. 10 and 11, when the water flow rate was lower than 2 mL/min, the appearing time of the channel flow was higher than 20 min and the disappearing time was higher than 106 min with decreasing water flow rate for all experimental conditions. When the water flow rate was lower than 1.0 mL/min, the change of appearing time and disappearing time of the flow channel was a nearly linear sudden increase. This indicated that the time for the appearance and disappearance of the flow channel is longer with a water flow rate lower than 0.1 mL/min under the same flow pressure, and it can be predicted that there will be no MH dissociation when the water flow rate is low enough. Similarly, when the water flow rate was 10.0 mL/min, the flow channel appearing times were 2, 4, and 14 min for pressures of 3200, 3300, and 6000 kPa, respectively, and the corresponding flow channel disappearing times

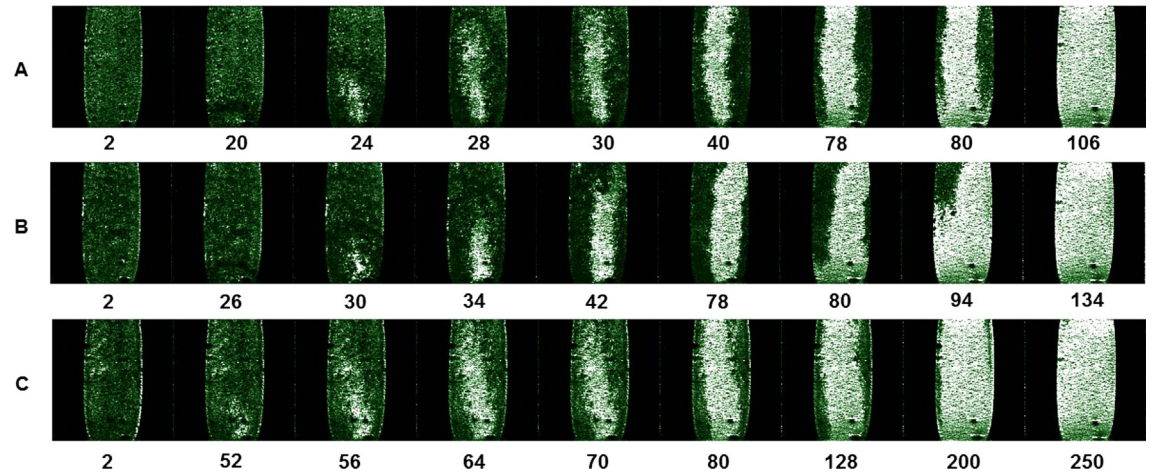

Fig. 6. Distribution changes for MH during water injection with a water velocity of 2.0 mL/min and under backpressures of 3200, 3300, and 6000 kPa.

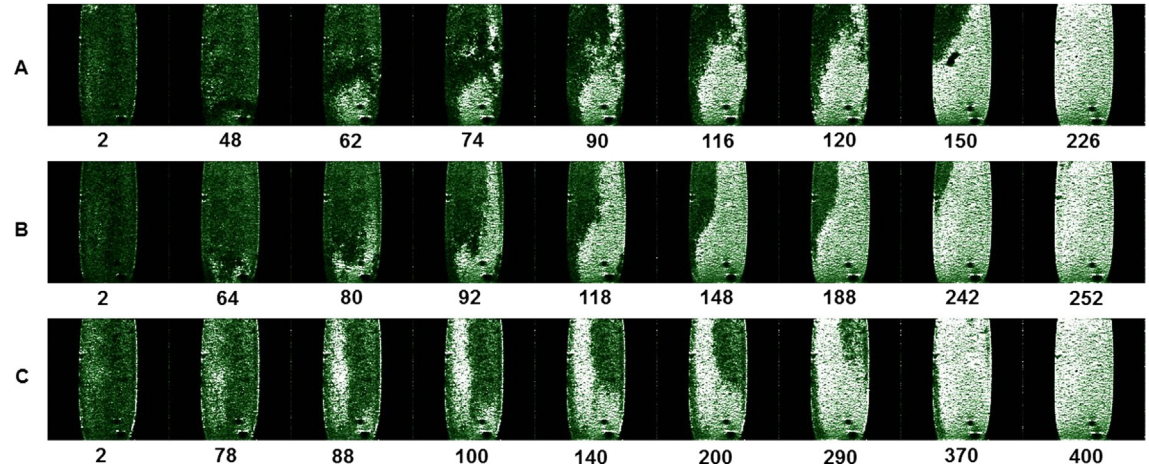

Fig. 7. Distribution changes for MH during water injection with a water velocity of 1.5 mL/min and under backpressures of 3200, 3300, and 6000 kPa.

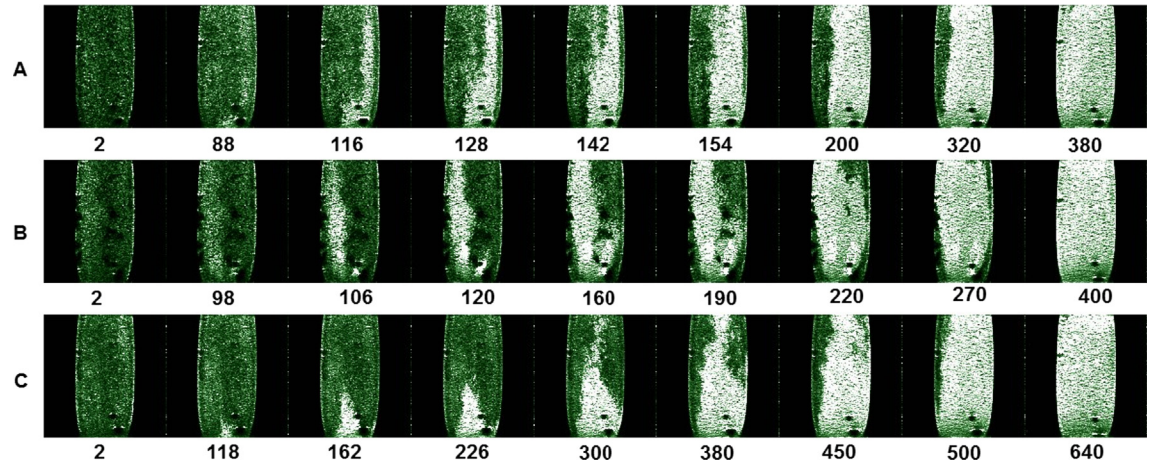

Fig. 8. Distribution changes for MH during water injection with a water velocity of 1.0 mL/min and under backpressures of 3200, 3300, and 6000 kPa.

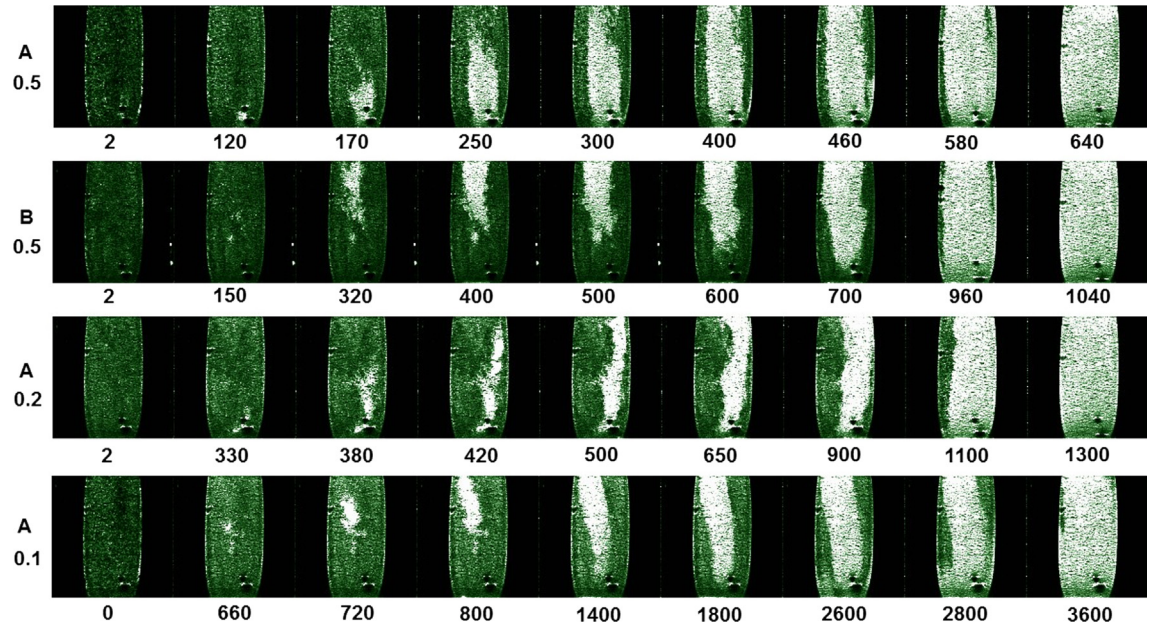

Fig. 9. Distribution changes for MH during water injection with water velocities of 0.5, 0.2, and 0.1 mL/min under backpressures of 3200 and 3300 kPa.

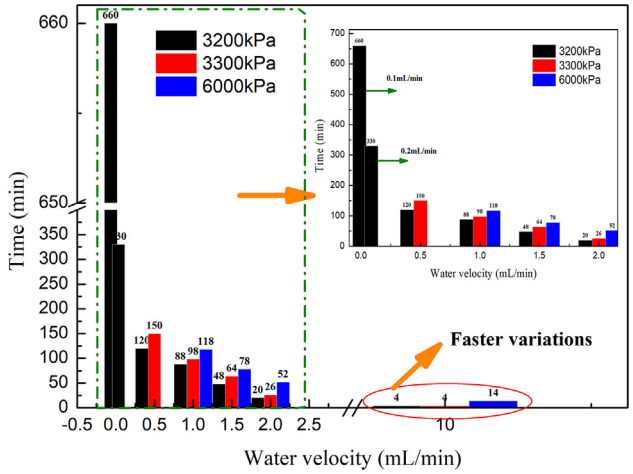

Fig. 10. Appearing time of flow channel during the continuous water flow process.

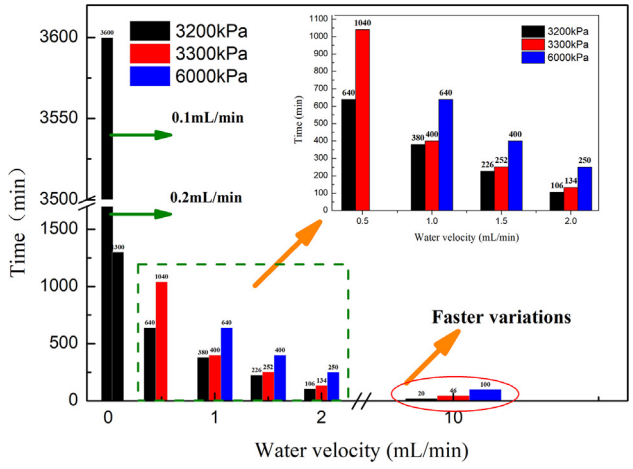

Fig. 11. Disappearing time of flow channel during the continuous water flow process.

were 20, 46, and 100 min. The flow pressure had a significant impact on the flow channel appearing and disappearing times, as shown in Figs. 10 and 11, respectively. The flow channel appearing time and disappearing time will become longer with increasing flow pressure. Thus, the flow channel appearing and disappearing times will increase with water flow rates higher than 0.1 mL/min under the same flow pressure, and it can be predicted that there will be no change in the flow channel appearing and disappearing times when the water flow rate is high enough.

In the oceans, there are huge reserves of seawater over hydrate accumulation areas. Thus, the problem of huge amount of water injection will be solved. Furthermore, hydrate exploitation can be carried out above the hydrate phase equilibrium, which will protect the environment around the hydrate reservoir during the process. However, depressurization is considered to be the most effective method for gas recovery from hydrate deposits [37,48]. There is a greater driving force for inducing hydrate decomposition in the initial period of hydrate exploitation. However, this driving force is not sufficient in the later period of hydrate exploitation by depressurization. Additionally, there is a higher water-gas permeability in the later period of hydrate exploitation by depressurization, which provides great conditions for water flow. Heat and mass transfer is the key factor for hydrate exploitation, and there will be a faster heat and mass transfer in the water flow erosion method, especially in the later period of hydrate exploitation by depressurization. Thus, the combination of water flow erosion with depressurization will be a greater method for hydrate exploitation. Furthermore, the water flow erosion method with a suitable water flow rate solves the problem of low driving force, and greatly improves the hydrate exploitation efficiency. Thus, there will be a huge potential for this method in the field production test.

4. Conclusion

The variation of MH distribution during the water flow process was investigated to contribute to the exploitation of hydrates. The results are summarized as follows:

(1) A visualization study on the distribution of hydrates in hydrate-bearing sediment during the water flow process was carried out. The influence of temperature and pressure variations on MH dissociation was eliminated completely in the experiments. The influence of water migration on MH dissociation was systematically analyzed.
(2) A new method of water flow erosion for natural gas hydrate (NGH) exploitation is proposed in this study. The investigation of water migration will be beneficial to hydrate exploitation in practical engineering. Combining this method with others will improve the efficiency of hydrate exploitation.
(3) The chemical potential difference between the hydrate phase and the aqueous phase caused MH dissociation during water flow process. The MH dissociation rate increased with decreasing back-pressure and increasing water flow rate. When the rate of MH dissociation is lower, it will take longer for the flow channel to appear, vary, and disappear.
(4) According to the trend of the variation of flow channel appearing time and disappearing time, it can be predicted that there will be no MH dissociation when the water flow rate is low enough, and there will be no change in the flow channel appearing and disappearing times when the water flow rate is high enough.

Acknowledgments

This project was financially supported by the National Key Research and Development Plan of China (Grant Numbers 2017YFC0307303, 2016YFC0304001), the National Natural Science Foundation of China (Grant Number 51576025, 51436003), and the Fundamental Research Funds for the Central Universities of China.

References

[1] Li X-S, Xu C-G, Zhang Y, Ruan X-K, Li G, Wang Y. Investigation into gas production from natural gas hydrate: a review. Appl Energy 2016;172:286–322.
[2] Song Y, Yang L, Zhao J, Liu W, Yang M, Li Y, et al. The status of natural gas hydrate research in China: a review. Renewable Sustainable Energy Rev 2014;31:778–91.
[3] Zhao J, Song Y, Lim X-L, Lam W-H. Opportunities and challenges of gas hydrate policies with consideration of environmental impacts. Renewable Sustainable Energy Rev 2017;70:875–85.
[4] Jr EDS, Koh CA. Clathrate hydrates of natural gases. Crc Press; 2008.
[5] Xu C-G, Li X-S. Research progress on methane production from natural gas hydrates. RSC Adv 2015;5:54672–99.
[6] Demirbas A. Methane hydrates as potential energy resource: Part 1 – importance, resource and recovery facilities. Energy Convers Manage 2010;51:1547–61.
[7] Zhao J, Liu D, Yang M, Song Y. Analysis of heat transfer effects on gas production from methane hydrate by depressurization. Int J Heat Mass Transfer 2014;77:529–41.
[8] Englezos P. Clathrate hydrates. Ind Eng Chem Res 1993;32:1251–74.
[9] Buffett BA. Clathrate Hydrates. Annu Rev Earth Planet Sci 2000;28:477–507.
[10] Holder GD, Corbin G, Papadopoulos KD. Thermodynamic and molecular properties of gas hydrates from mixtures containing methane, argon, and krypton. Ind Eng Chem Fundam 1980;19:282–6.
[11] Ji C, Ahmadi G, Smith DH. Natural gas production from hydrate decomposition by depressurization. Chem Eng Sci 2001;56:5801–14.
[12] Holder, G, Angert P. Simulation of gas production from a reservoir containing both gas hydrates and free natural gas, In: SPE Annual Technical Conference and Exhibition; 1982.
[13] Moridis, GJ, Kowalsky M. Depressurization-induced gas production from Class 1 and Class 2 hydrate deposits; 2006.

[14] Zhao J, Zhu Z, Song Y, Liu W, Zhang Y, Wang D. Analyzing the process of gas production for natural gas hydrate using depressurization. Appl Energy 2015;142:125–34.
[15] Schicks J, Spangenberg E, Giese R, Luzi-Helbing M, Priegnitz M, Beeskow-Strauch B. A counter-current heat-exchange reactor for the thermal stimulation of hydrate-bearing sediments. Energies 2013;6:3002–16.
[16] Ota M, Abe Y, Watanabe M, Smith Jr. RL, Inomata H. Methane recovery from methane hydrate using pressurized CO2. Fluid Phase Equilib 2005;228–229:553–9.
[17] Koh D-Y, Kang H, Lee J-W, Park Y, Kim S-J, Lee J, et al. Energy-efficient natural gas hydrate production using gas exchange. Appl. Energy 2016;162:114–30.
[18] Li Y, Liu W, Zhu Y, Chen Y, Song Y, Li Q. Mechanical behaviors of permafrost-associated methane hydrate-bearing sediments under different mining methods. Appl. Energy 2016;162:1627–32.
[19] Li G, Li X-S, Tang L-G, Zhang Y. Experimental investigation of production behavior of methane hydrate under ethylene glycol injection in unconsolidated sediment. Energy Fuel 2007;21:3388–93.
[20] Li G, Wu D-M, Li X-S, Lv Q-N, Li C, Zhang Y. Experimental measurement and mathematical model of permeability with methane hydrate in quartz sands. Appl Energy 2017;202:282–92.
[21] Yousif MH. Effect of underinhibition with methanol and ethylene glycol on the hydrate-control. Process 1998.
[22] Oyama H, Konno Y, Masuda Y, Narita H. Dependence of depressurization-induced dissociation of methane hydrate bearing laboratory cores on heat transfer. Energy Fuel 2009;23:4995–5002.
[23] Li G, Wu D, Li X, Zhang Y, Lv Q, Wang Y. Experimental investigation into the production behavior of methane hydrate under methanol injection in quartz sand. Energy Fuel 2017;31:5411–8.
[24] Yousif M, Abass H, Selim M, Sloan E. Experimental and theoretical investigation of methane-gas-hydrate dissociation in porous media. SPE Reservoir Eng 1991;6:69–76.
[25] Yousif M, Li P, Selim M, Sloan E. Depressurization of natural gas hydrates in Berea sandstone cores. J Inclusion Phenom Mol Recognit Chem 1990;8:71–88.
[26] Kono HO, Narasimhan S, Song F, Smith DH. Synthesis of methane gas hydrate in porous sediments and its dissociation by depressurizing. Powder Technol 2002;122:239–46.
[27] Moridis GJ, Sloan ED. Gas production potential of disperse low-saturation hydrate accumulations in oceanic sediments. Energy Convers Manage 2007;48:1834–49.
[28] Konno Y, Masuda Y, Hariguchi Y, Kurihara M, Ouchi H. Key factors for depressurization-induced gas production from oceanic methane hydrates. Energy Fuel 2010;24:1736–44.
[29] Kawamura T, Ohga AK, Higuchi K, Yoon JH, Yamamoto Y, Komai AT, et al. Dissociation behavior of pellet-shaped methane – ethane mixed gas hydrate samples. Energy Fuels 2003;17:614–8.
[30] Tang LG, Rui X, Chong H, And ZPF, Fan SS. Experimental investigation of production behavior of gas hydrate under thermal stimulation in unconsolidated sediment. Chin J Process Eng 2005;19:2402–7.
[31] Su Z, Cao Y, Wu N, He Y. Numerical analysis on gas production efficiency from hydrate deposits by thermal stimulation: application to the Shenhu area, South China Sea. Energies 2011;4:294–313.
[32] Komai T, Kawamura T, Kang S, Nagashima K, Yamamoto Y. In situ observation of gas hydrate behaviour under high pressure by Raman spectroscopy. J Phys: Condens Matter 2002;14:11395.
[33] Geng CY, Wen H, Zhou H. Molecular simulation of the potential of methane reoccupation during the replacement of methane hydrate by CO(2). J Phys Chem A 2009;113:5463–9.
[34] Mutalik PN, Mutalik PN. Experimental study of brine injection and depressurization methods for dissociation of gas hydrates. SPE Formation Eval 1991;6:477–84.
[35] Li X, Wan L, Li G, Li Q, Chen Z, Yan K. Experimental investigation into the production behavior of methane hydrate in porous sediment with hot brine stimulation. Ind Eng Chem Res 2008;47:9–11.
[36] Chong ZR, Pujar GA, Yang M, Linga P. Methane hydrate formation in excess water simulating marine locations and the impact of thermal stimulation on energy recovery. Appl Energy 2016;177:409–21.
[37] Chong ZR, Yin Z, Tan JHC, Linga P. Experimental investigations on energy recovery from water-saturated hydrate bearing sediments via depressurization approach. Appl Energy 2017;204:1513–25.
[38] Chong ZR, Zhao J, Chan JHR, Yin Z, Linga P. Effect of horizontal wellbore on the production behavior from marine hydrate bearing sediment. Appl Energy 2018;214:117–30.
[39] Chong ZR, Yang SHB, Babu P, Linga P, Li X-S. Review of natural gas hydrates as an energy resource: prospects and challenges. Appl Energy 2016;162:1633–52.
[40] Li B, Li X-S, Li G, Jia J-L, Feng J-C. Measurements of water permeability in unconsolidated porous media with methane hydrate formation. Energies 2013;6:3622–36.
[41] Yang M, Song Y, Jiang L, Wang X, Liu W, Zhao Y, et al. Dynamic measurements of hydrate based gas separation in cooled silica gel. J Ind Eng Chem 2014;20:322–30.
[42] Yang M, Song Y, Liu W, Zhao J, Ruan X, Jiang L, et al. Effects of additive mixtures (THF/SDS) on carbon dioxide hydrate formation and dissociation in porous media. Chem Eng Sci 2013;90:69–76.
[43] Sean W-Y, Sato T, Yamasaki A, Kiyono F. CFD and experimental study on methane hydrate dissociation Part I. Dissociation under water flow. AIChE J 2007;53:262–74.
[44] Liu W, Wu Z, Li Y, Song Y, Ling Z, Zhao J, et al. Experimental study on the gas phase permeability of methane hydrate-bearing clayey sediments. J Nat Gas Sci Eng 2016;36:378–84.
[45] Mori YH, Mochizuki T. Mass transport across clathrate hydrate films — a capillary permeation model. Chem Eng Sci 1997;52:3613–6.
[46] Selim MS, Sloan ED. Heat and mass transfer during the dissociation of hydrates in porous media. Aiche J 1989;35:1049–52.
[47] Wang Y, Feng J-C, Li X-S, Zhang Y, Li G. Analytic modeling and large-scale experimental study of mass and heat transfer during hydrate dissociation in sediment with different dissociation methods. Energy 2015;90:1931–48.
[48] Wang Y, Feng J-C, Li X-S, Zhang Y. Experimental and modeling analyses of scaling criteria for methane hydrate dissociation in sediment by depressurization. Appl Energy 2016;181:299–309.
[49] Wang Y, Feng J-C, Li X-S, Zhang Y, Chen Z-Y. Fluid flow mechanisms and heat transfer characteristics of gas recovery from gas-saturated and water-saturated hydrate reservoirs. Int J Heat Mass Transfer 2018;118:1115–27.
[50] Song Y, Wang S, Jiang L, Zhang Y, Yang M. Hydrate phase equilibrium for CH4-CO2-H2O system in porous media. Can J Chem Eng 2016;94:1592–8.
[51] Yang L, Falenty A, Chaouachi M, Haberthür D, Kuhs WF. Synchrotron X-ray computed microtomography study on gas hydrate decomposition in a sedimentary matrix. Geochem Geophys Geosyst 2016.